Journal of Materials Chemistry A

Accepted Manuscript

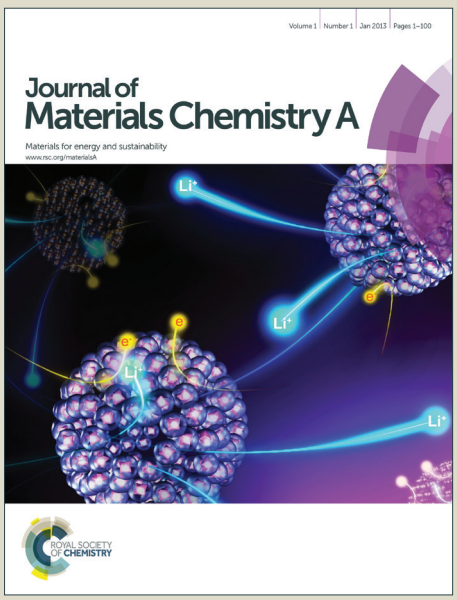

ROYAL SOCIETY OF CHEMISTRY

www.rsc.org/materialsA

Journal Name

RSCPublishing

ARTICLE

Intriguing differences in hydrogen adsorption in CPO-27 materials induced by metal substitution

Cite this: DOI: 10.1039/x0xx00000x

Received 00th January 2012,
Accepted 00th January 2012

DOI: 10.1039/x0xx00000x

www.rsc.org/

Mali H. Rosnes,[a] Martin Opitz,[a,†] Matthias Frontzek,[b] Wiebke Lohstroh,[c] Jan Peter Embs,[b] Peter A. Georgiev,[d,e]* Pascal D. C. Dietzel[a,]*

An extraordinarily interesting series of metal-organic framework compounds are the isostructural microporous coordination polymers [M_2(dhtp)] (CPO-27-M, M-MOF-74 or M_2(dobdc)) in which a high concentration of coordinatively unsaturated metal sites results in high initial heats of adsorption for a variety of adsorbents. We present here a comparative study of hydrogen gas adsorption experiments on CPO-27-Cu and -Mn, which show significant differences in their hydrogen uptake behaviours which can be attributed to the difference in interaction between hydrogen and the respective metal cation incorporated in the framework structure. Inelastic neutron scattering and neutron diffraction experiments were carried out to gain additional insight into the adsorption processes leading to the difference in hydrogen uptake behaviour by the two compounds. On the basis of the experimental results the hydrogen uptake properties of CPO-27-Cu and -Mn are compared, and finally related to the properties of the other members of the CPO-27 series. It is found that CPO-27-Cu demonstrates the lowest isosteric heat of adsorption for H_2 of all the CPO-27-M materials reported to date, where M = Ni, Co, Mg, Zn, Mn, and Fe, whereas CPO-27-Mn demonstrates the second lowest. While all the previously reported CPO-27 materials show two steps in the adsorption isotherm and two distinct values corresponding to the first and second adsorption sites in the heats of adsorption, these are not observed for CPO-27-Cu. Consequently, the open metal site and the second adsorption site are energetically equivalent, and there is no preference for the hydrogen gas at the open metal centre.

Introduction

Coordination polymers (CPs) or metal-organic frameworks (MOFs) are infinite networks consisting of metal centres linked by organic ligands. They are intensely studied for their wide variety of potential applications due to structural diversity. MOFs are frequently porous with high specific surface areas which enable application ranging from gas storage and separation to heterogeneous catalysis.[1-3] The isostructural series CPO-27-M, (Figure 1) also denoted M_2(dhtp), M_2(dobdc) (dhtp / dobdc = $C_8H_2O_6^{4-}$) or M-MOF-74, where M = Co,[4] Ni,[5] Mg,[6] Mn,[7] Zn,[8] Fe[9,10] and Cu,[11,12] is potentially one of the most

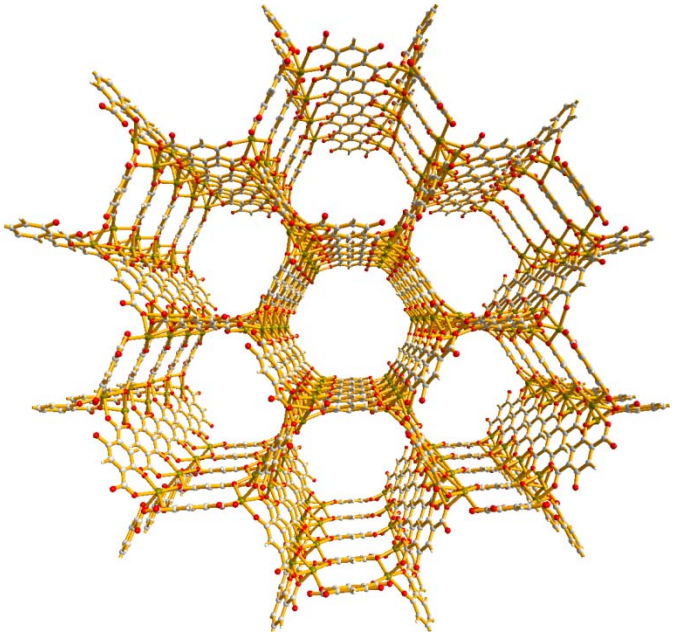

Figure 1: The dehydrated structure of CPO-27-M.

[a]Department of Chemistry, University of Bergen, P.O. Box 7803, N-5020 Bergen, Norway. E-mail: Pascal.Dietzel@kj.uib.no
[b]Laboratory for Neutron Scattering and Imaging, Paul Scherrer Institut, CH-5232 Villigen, Switzerland
[c]Heinz Maier-Leibnitz Zentrum (MLZ), Technische Universität München, Lichtenbergstraße 1, D-85748 Garching, Germany
[d]Department of Chemistry, University of Milan, 21 Via Golgi, I-20133 Milan, Italy. E-mail: pageorgiev@yahoo.co.uk
[e]Faculty of Chemistry and Pharmacy, University of Sofia, James Bourchier 1, 1164 Sofia, Bulgaria
[†]Current address: Institute of Physical Chemistry, University of Marburg, Hans-Meerwein-Straße, D-35032 Marburg, Germany.
† Electronic Supplementary Information (ESI) available. See DOI: 10.1039/b000000x/

interesting CP families for application in adsorption and separation processes due to their high concentration of open metal sites, combined with a stable and rigid open framework structure. The structure is based on a honeycomb design with internal pores of about 1.2 nm in diameter. The metal cations are in an octahedral coordination with six oxygen atoms, where one of the six oxygen atoms is part of a solvent molecule. This solvent molecule is easily removed, leaving the metal centre in a square-pyramidal coordination with the non-occupied sixth coordination site available for interaction with adsorptives (this construct being called open metal site).[4,13] The presence of open metal sites leads to higher gas storage capacities at lower pressures and also better selective gas adsorption from gas mixtures.[5,14-17] The open metal sites in CPO-27 have been confirmed as the primary location for adsorbed gas molecules by both X-ray and neutron diffraction studies.[7,13,18-27] Due to the open metal sites the CPO-27 materials are particularly interesting for gas uptake, and one of the pertinent gasses is hydrogen.[7,18] Hydrogen is heavily investigated as carrier for energy obtained from greener sources.[28-30] Albeit the huge potential in applications such as hydrogen fuel cells, there are still challenges concerning storage and transportation of hydrogen.

For the potential hydrogen storage in porous materials, hydrogen affinity is important, usually quantified as the isosteric heat of adsorption, Q_{st}. Due to the open metal sites available in CPO-27 materials these are some of the best candidates among MOFs. Hydrogen sorption in CPO-27-M materials has been extensively studied for M = Ni,[5,25] Co,[7] Mg,[7] Zn,[14,31] Mn[7,27] and Fe.[10,32] However, there is no data yet available on CPO-27-Cu. The nitrogen and hydrogen isotherms previously reported for the different members of the isostructural CPO-27 series all follow very similar trends, but with a varying degree of available specific surface area, pore volume and gas uptake properties due to the difference in formula weight along the series. The largest amount of hydrogen adsorbed at 100 kPa and 77 K has been reported for CPO-27-Mg, the lightest compound in the series. It reaches a hydrogen uptake of 2.5 wt%.[18] The most evident feature for the series is the initial steep gas uptake observed in the isotherms, which for hydrogen sorption data usually occurs below 5 kPa at 77 K. It corresponds to the occupation of the primary adsorption site on the framework, which has been confirmed to happen at the open metal site for a variety of gases such as hydrogen, carbon dioxide, nitrogen monoxide, and methane.[33] Thereafter, the adsorption isotherm continues with a less steep slope, hence the second molecule of hydrogen is adsorbed over a pressure range more than 100 times larger than the range it took for the first molecule. This second adsorption site has been reported to be located directly above a triangle of oxygen atoms within the framework.[19] This two-step mechanism is especially evident when looking at the semi-logarithmic plot of the hydrogen isotherms, as demonstrated for CPO-27-Ni in Figure 2. The conclusion of previous works has been that the two adsorption positions are not equivalent and that adsorbed hydrogen molecules favour the open metal site over the alternative adsorption site.[18]

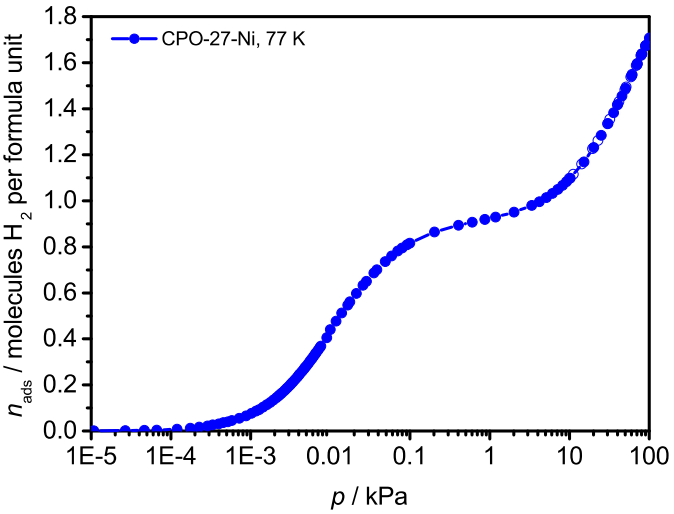

Figure 2: Reference isotherm showing two step hydrogen adsorption for CPO-27-Ni, in a semi-logarithmic plot.[18]

In accordance with the observed isotherms, the isosteric heats of adsorption for the different CPO-27 materials reported in the literature show two different plateaus, clearly indicating hydrogen adsorption preference at the open metal site over the second adsorption site. CPO-27-Ni has the strongest initial isosteric heat of adsorption for hydrogen of 13 kJ mol^{-1},[18] followed by decreasing values for Co (11.5 kJ mol^{-1}),[18] then Mg (10.9 kJ mol^{-1}),[18] Fe (9.5-10 kJ mol^{-1}),[10] Zn (8.8 kJ mol^{-1})[14,19] and finally Mn (8.8 kJ mol^{-1}).[7,27] It drops to 5-6 kJ mol^{-1} for all members of the series when reaching one molecule of hydrogen adsorbed per formula unit. As one would expect, based on the uniform chemical environment at the second adsorption site, the isosteric heat of adsorption is more or less equal for all members of the CPO-27 series, and the values observed correspond well with values typically observed for hydrogen adsorption on MOFs without open metal sites.

The CPO-27-Mn material, with detailed hydrogen sorption data and isosteric heat of hydrogen adsorption, has been reported previously.[7,27] Recently, Geier et al. also reported the structure of the empty CPO-27-Mn material based on neutron powder diffraction data.[34] However, structural data when loaded with hydrogen or deuterium (such as neutron diffraction or INS) have not yet been reported for the manganese analogue. Hence, herein we report a comparative study of high precision hydrogen sorption data for the CPO-27-Cu and CPO-27-Mn. Additionally, the Mn analogue, with the lowest isosteric heat of hydrogen adsorption reported to date, is particularly suited to illustrate the change in behaviour of the copper compound in comparison to the other members of the series in light of the results presented herein for CPO-27-Cu. Both compounds are carefully analysed and compared to the previously reported members of the CPO-27 series.

It was uncertain if it would be possible to insert Cu(II) into the CPO-27 series due the Jahn-Teller effect. However, recent

reports by Sanz *et al.*[12] and our own synthetic procedure reported herein show that CPO-27-Cu can be successfully synthesised. We characterised the compound by powder X-ray diffraction, thermogravimetric analysis and differential scanning calorimetry, elemental analysis, SEM and nitrogen adsorption. To allow for better comparison of the hydrogen sorption properties to all the other CPO-27 materials, we also carried out hydrogen gas adsorption and *in situ* neutron scattering experiments on CPO-27-Mn and -Cu, shedding new light on how the nature of the metal affects the hydrogen uptake properties of the CPO-27 materials. In contrast to sorption measurements, neutron scattering techniques allow for a detailed microscopic view on individual adsorption sites in the studied host materials. It provides a detailed insight into how adsorbed hydrogen molecules interact with the internal surface area of the Cu analogue compared to the other CPO-27-M materials.

Experimental

Instrumentation

Scanning electron microscopy (SEM): *ZEISS Supra 55VP* scanning electron microscope. Filament: field emission. KV range: 100 V to 30 kV. STEM detector, EDX detector for element analyses, WDS detector for element analyses, backscatter detector, cathode luminescence detector and variable pressure detector. **Elemental Analysis (EA):** CHN analyses were carried out on an *Elementar vario EL III*. **Thermo Gravimetric Analysis - Differential Scanning Calorimeter (TG-DSC):** *Netsch Jupiter STA 449 F1* (TGA-DSC) was used. **Powder X-ray diffraction (PXRD):** PXRD was carried out on a *Bruker AXS D8 Advance*, with a 9 position multisampler. Data collection was performed using monochromatic Cu Kα_1 radiation in Bragg-Brentano geometry. **Gas adsorption:** The gas adsorption measurements were carried out on a *BELSORP-max* instrument equipped with a low pressure transducer and a turbomolecular pump, allowing measurements from very low pressures ($p/p_0 = 10^{-8}$) and high precision. The samples were prepared under inert conditions and transferred to the sample cell in a glove box. Prior to the measurements the samples of CPO-27-Mn and CPO-27-Cu were activated at 200 °C and 120 °C, respectively, for 24 hours in a dynamic vacuum. **Inelastic Neutron Scattering (INS):** Inelastic Neutron Scattering experiments of *in situ* dosed dihydrogen were performed on the FOCUS[35] instrument at the SINQ neutron source at the Paul Scherer Institute in Villigen, Switzerland, for CPO-27-Mn, and on the TOF TOF spectrometer[36] at the FRM II neutron source, in Garching, Germany, for CPO-27-Cu. Pre-evacuated amounts of 1.47 g for the Cu compound and 1.11 g for the Mn compound were loaded in Al-scattering cells using a He-filled glove bag. Prior to the INS measurements the samples were additionally evacuated for 6 hours at 120 and 180 °C, respectively. Neutrons with wavelengths of 2.0 Å and 1.8 Å were used for the CPO-27-Mn and Cu samples, accordingly, resulting in energy resolutions of about 0.8 and 1.2 meV. **Neutron Diffraction:** Desolvated CPO-27-Mn and CPO-27-Cu samples were measured on the HRPT[37] instrument (neutron wavelength 1.886 Å). Desolvated and *in situ* D_2 dosed CPO-27-Mn and CPO-27-Cu samples were measured on the DMC[38] instrument (neutron wavelength 2.45 Å). Both instruments are installed at the SINQ neutron source, PSI, Villigen, Switzerland. 1.02 g of desolvated CPO-27-Mn and 0.40 g of desolvated CPO-27-Cu were loaded in a vanadium sample containers of 8 mm diameter each, and attached to a centre stick equipped with a gas capillary, using a He-filled glove bag. Prior to the neutron measurements the samples were additionally evacuated at 180 °C and 120 °C, respectively, for 12 hours. Diffraction patterns of the fully activated materials were measured on the HRPT and DMC instruments at 1.5 and 20 K. D_2 dosing procedures were performed using a custom built Sievert's type volumetric rig, at 70 K, 50 K, and 45 K, accordingly. Equilibration periods of 20 min were applied at each point.

Structure refinements were performed with the use of the Fullprof suite of programs.[39] The refinement results of the HRPT wide angle data were used as starting point for the DMC data refinements, in which the atomic thermal factors of the framework were fixed. All other parameters, including all atom coordinates and deuterium thermal factors, as well as peak shape parameters were refined for all DMC data. Because of its nearly free rotational state, precluding accurate refinement of the D–D bond length and orientation, each D_2 molecule was introduced as a single deuteron with double site occupancy and shape and size taken into account by the corresponding thermal factors. The corresponding refinement plots for the data of the two materials with 0, 0.5, 1, and 1.8/2 (Cu/Mn, respectively) D_2 per M(II) centre are shown in Figures S5-14, and the corresponding unit cell parameters are summarised in Table S5. **DFT Calculations:** Quantum chemical model calculations of the thermodynamics of H_2 binding in the two CPO-27 materials were performed within the frame of the Density Functional Theory (DFT) and the Generalize Gradient Approximation (GGA), Perdew-Berke-Ernzernhof (PBE) functional with the Projector Augmented Wave (PAW) formalism, as implemented in the ABINIT v.7 software.[40,41,41] Full geometry optimisations of the corresponding rhombohedral primitive unit cells containing zero H_2, 6 H_2 and 12 H_2 molecules per primitive unit cell for the desolvated materials were carried out, where 6 H_2 in the primitive unit cell corresponds to 1 H_2 per metal centre and 12 H_2 to 2 H_2 per metal centre. In each case we used 816 meV energy cut off on the plane wave basis, and a 1×1×2 Monkhorst-Pack *k* point mesh. To ensure high spin state of Mn(II), spin polarised calculations were performed for the Mn structure, assuming an antiferromagnetic order in which Mn(II) spins within one -O-M-O- chain aligned in parallel, but the interchain order is antiparallel. This was not necessary for the CPO-27-Cu structure and only spin unpolarised calculations were done. Geometry convergence criteria were set to 1 meV $Å^{-1}$ for each structure optimisation. The corresponding energy convergence was of the order of 10^{-8} meV. For the loading of 1 H_2 per metal centre, the H_2 binding energy was calculated as

the difference between the total energy of the fully optimised corresponding structure with H_2, minus the sum of the total energies of the fully optimised desolvated cell and the isolated H_2 molecule placed in the same unit cell size and shape as of the host structure. This latter energy appeared identical to the one obtained for H_2 in a box of 16×16×16 Å^3. The binding energy on the second set of adsorption sites was calculated with respect to the total energy of the unit cell loaded with 1 H_2 per metal centre. This provides good estimation of the individual site energies, assuming that the H_2-H_2 intersite interactions are much smaller compared to the interactions with the substrate. Dispersion interactions were additionally taken into account using the empirical correction of Grimme.[42] We optimised the coordinates of the adsorbed H_2 molecules only and recalculated the total energy of the optimised at the pure PBE level empty structure including the Grimme correction to recalculate the corresponding binding energy including dispersion interactions.

Materials

All chemicals, reagents and solvents were purchased from Sigma Aldrich and used as received without further purification. CPO-27-Cu and CPO-27-Mn were both synthesised under solvothermal conditions, and processed under inert conditions. The gases used for gas adsorption measurements were of 99.9995%, or higher, purity and were purchased from Yara Praxair.

Preparation of [Cu(C_4HO_3)]·4H_2O (CPO-27-Cu)

A mixture of 2,5-dihydroxyterephthalic acid (0.991 g, 5.0 mmol), 1,4-diazabicyclo[2.2.2]octane (DABCO, 0.280 g, 2.5 mmol) and copper(II) nitrate hemi(pentahydrate) (2.326 g, 10.0 mmol) in *N*,*N*-dimethylformamide (DMF, 60 mL) were stirred for 10 min in a Teflon-lined insert (125 mL volume). The insert was placed in an autoclave, sealed and reacted for 3 days at 60 °C in a preheated furnace. Filtration under inert conditions resulted in a very dark reddish-brown crystalline material consisting of very fine needle shaped crystals. The material was washed with DMF before the supernatant solvent was replaced by methanol three times, leaving each portion to stand for about 30 min, before it was filtered in a Schlenk apparatus. Samples for EA, PXRD and TG analyses were extracted before the sample was dried at 120 °C for 24 h in a dynamic vacuum. Yield [Cu(C_4HO_3)] 0.379 g (23.6 % based on Cu). Powder X-ray diffraction confirms the identity of the compound (Figure S2). EA: $C_4H_9CuO_7$ (232.66 g mol^{-1}): Calcd. C 20.65, H 3.90; found C 20.55, H 3.58. TGA: The first 29.85 % weight loss at below 100 °C can be accounted for by solvent associated with the compound (Figure S3). The weight loss starting at 150 ˚C of 39.02 % corresponds to the loss of all the organic material present, whilst the remaining 30.87 % corresponds to the residual CuO, as confirmed by PXRD analysis. EA and TG analyses indicate between 3 and 4 water molecules per formula unit.

Preparation of [Mn(C_4HO_3)]·4H_2O (CPO-27-Mn)

2,5-dihydroxyterephthalic acid (1.486 g, 7.5 mmol) was dissolved in NMP (80 mL) in a Teflon-lined insert (200 mL volume). A solution of manganese(II) acetate tetrahydrate (3.676 g, 15.0 mmol) in H_20 (10 mL) were added, and the insert was placed in an autoclave, sealed and reacted for 24 h at 110 °C in a preheated furnace. Filtration in a Schlenk apparatus yielded orange-red material and a little amount of colourless precipitate. The material was washed with copious amounts of water during which the main component changed its colour to orange and the colourless substance dissolved and washed away and subsequently with methanol (colour change to dark-orange) under inert conditions. The substance was left to stand under methanol for three days, during which the methanol was decanted and replaced once per day, before it was dried at 200 °C in dynamic vacuum. Yield: 2.009 g (88%). Accessibility of the void volume was confirmed by nitrogen gas adsorption, see right hand side of Figure S1.

Results and discussion

Synthesis and initial characterisation

The CPO-27-Cu material was synthesised using the solvothermal synthesis technique. After 3 days at 60 °C the material was collected by filtration under inert conditions. Using an optical microscope very small, fine and intertwined dark reddish-brown needle shaped crystals were observed at high magnification (115x). Scanning electron microscopy (SEM) was carried out on the material, and the results can be seen in Figure 3. From the detailed SEM image it is evident that the material actually consists of individual crystals of hexagonal rod shape. The hexagonal rod shape is very homogenous throughout all the different samples we investigated by SEM, but as can been seen in Figure 3 the crystals vary in size within each sample. The shape of the crystals is as expected for CPO-27 materials with their hexagonal channel structure.

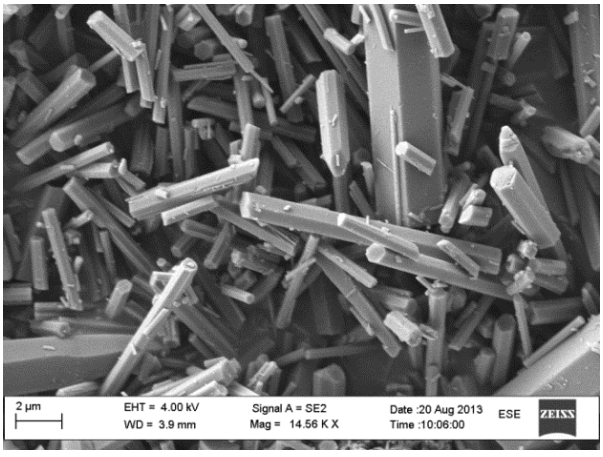

Figure 3: SEM image showing the crystal shape and size distribution of CPO-27-Cu.

The identity and purity of the material was confirmed by performing a Pawley fit of the powder X-ray diffraction pattern,

from which we obtained lattice parameters (rhombohedral space group $R\bar{3}$, $a = b = 26.1268(5)$ Å, $c = 6.3270(3)$ Å, $\alpha = \beta = 90$ °, $\gamma = 120$ °, V = 3740.28(23) Å^3), corresponding well to the values of the reported single crystal structure determination.[5] Remarkably, we have discovered that the presence of the base 1,4-diazabicyclo[2.2.2]octane (DABCO) improves the synthesis of the pure CPO-27-Cu material, even though it is not incorporated in the metal-organic framework structure. Alternative synthetic approaches using other bases such as sodium hydroxide and triethylamine were attempted, but it was quickly realised that at least at the relatively low reaction temperature we have employed, DABCO is a prerequisite for the successful synthesis of the phase pure material. The analyses carried out on the CPO-27-Cu also confirm that there are no traces of DABCO in the final product. The yield of the CPO-27-Cu synthesis reported herein is generally around 23 %, which is significantly below the yields we obtain for the other CPO-27 materials whose syntheses are typically run at higher temperatures. We have observed that the yield can be significantly improved by increasing the concentration of the reactants, but unknown impurities appeared and the nitrogen gas uptake was severely reduced for the product obtained. In summary, by fine tuning the reaction parameters such as the temperature, reaction time, concentration and ratio of metal salt *vs*. the organic ligand, and finally the ratio of DABCO, we obtained a reproducible and reliable experimental procedure resulting in pure, well-defined needle shaped crystals.

The porosity of the material was confirmed by nitrogen sorption measurements at 77 K (Figure S1). Based on the nitrogen adsorption data the Langmuir specific surface area was determined to be 1422 m^2 g^{-1}. Using BET calculations the specific surface area was found to be 1369 m^2 g^{-1}, where the criteria suggested by Rouquerol *et al.* was used to aid in the identification of the linear region of the nitrogen isotherm for the BET calculation.[43,44] The total pore volume was found to be 0.50 cm^3 g^{-1} at $p/p_0 = 0.5$. The BET specific surface area is higher compared to the previously reported data for CPO-27-Cu, which could be due to the fact that our material was treated under inert conditions. The pore volume agrees well with the values obtained for the other CPO-27 materials and calculations on the basis of the isostructural CPO-27-Ni (using the calculated void space function of PLATON or Mercury's void), indicating that we have managed to obtain a phase pure material with full access to its porosity. The values of CPO-27-Mn also correspond to the expectations for its textural properties.

Hydrogen sorption

Hydrogen adsorption experiments for the copper and manganese analogues of CPO-27 measured at 77 and 87 K are compared in Figure 4. As previously mentioned, the main differences between the members of the CPO-27 series are the slope of the initial uptake (related to the metal-dependent specific pressure at which it occurs), the level at which it slows down, and finally the amount of adsorbed hydrogen. The hydrogen isotherm for CPO-27-Mn measured at 77 K follows the same trend as the rest of the series, with an initial steep gas uptake before it levels off near 1 H_2 per Mn. However, the initial steep uptake is not as steep as the values reported for M = Ni, Co, Mg nor Fe, indicating that the first interaction between open metal site and adsorptive is generally weaker for CPO-27-Mn. Literature data for CPO-27-Zn shows that the initial uptake in the adsorption isotherms for CPO-27-Mn and -Zn are very similar,[19] however the first interaction between the open metal site and the adsorptive is still weaker for CPO-27-Mn.

The hydrogen uptake for CPO-27-Mn of 1.92 wt% at 77 K and 100 kPa (1.57 wt% at 87 K) is lower than what has been reported for the other CPO-27 members The slope of the hydrogen isotherm obtained for CPO-27-Cu at 77 K is even more gradual compared to that of the CPO-27-Mn analogue, indicating that the strength of interaction between the material and hydrogen has diminished further. The hydrogen uptake in CPO-27-Cu was measured to be as low as 1.46 wt% at 77 K and 100 kPa (1.05 wt% at 87 K). The difference in the hydrogen isotherms, particularly for the first adsorption step, between that observed for the copper and the manganese analogues is even clearer when looking at the slope of the data obtained at 87 K below 20 kPa, see Figure 4.

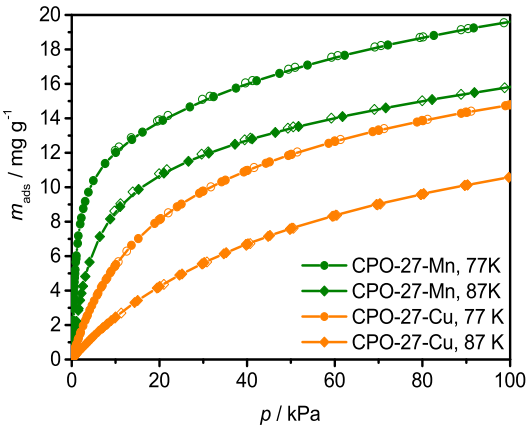

Figure 4: Hydrogen isotherm for CPO-27-Cu (in orange) and CPO-27-Mn (in green). The adsorption branch is shown as filled symbols, whilst the desorption branch is shown as empty symbols.

The two-step hydrogen adsorption mechanism is more prominent when looking at the semi-logarithmic plots of the isotherms and a comparison of the isotherms for the nickel, cobalt, magnesium, iron, manganese and copper versions is shown in Figure 5. The trend observed here is similar to the one discussed above, with the Ni analogue (in blue) as the extreme in the series, where the first adsorption step, the filling of the open metal site, occurs well below 1 kPa. This is at a lower pressure compared to the other members and reflects the fact that the Ni(II) cation has the strongest interaction between adsorption site and hydrogen. The Co (pink), Mg (red), and Fe (olive) analogues display similar isotherms in which the initial uptake is shifted to consecutively slightly higher pressure

compared to that for the Ni analogue. A more significant difference is observed when we move on to the isotherm displayed by the Mn analogue (green). The first molecule of hydrogen is again adsorbed at a higher pressure compared to the previously discussed cases, and the two sigmoid steps can only be identified on close inspection indicating there is less of an energy difference between the first and the second adsorption site in CPO-27-Mn. However, the most significant difference is observed for the CPO-27-Cu material (orange), where the semi-logarithmic plot of the isotherm is notably different from all the other CPO-27 materials. The isotherm is a smooth curve without any visible steps, and the adsorption only starts at pressures around 1 kPa, which is much higher than for any other CPO-27 analogue. Apparently the open metal site (site I) and the second adsorption site (site II) have nearly the same affinity for hydrogen molecules in this case. As a consequence, one would expect both sites to be filled roughly simultaneously upon adsorption of hydrogen. This is in contrast to all the other reported CPO-27 materials for which the two sites are filled sequentially. In summary, Figure 5 shows how the first adsorption plateau moves towards higher pressures with the decrease of the Q_{st} for the different metals cations, until it finally merges with the second adsorption plateau for the Cu analogue.

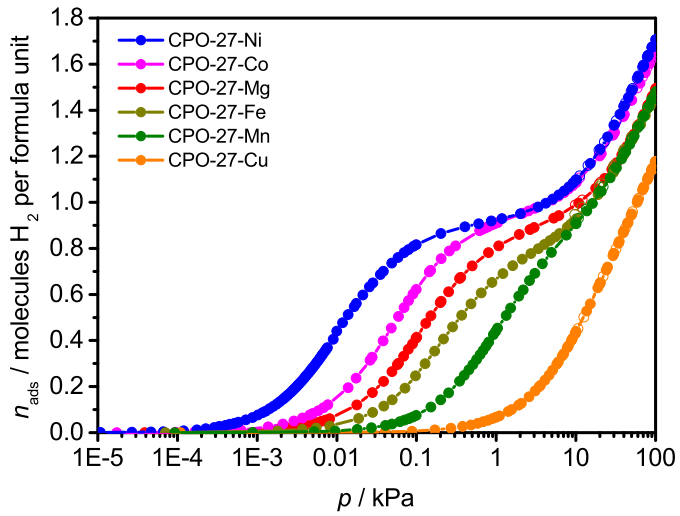

Figure 5: Comparison of hydrogen uptake for CPO-27-M at 77 K, where M = Ni (blue), Co (pink), Mg (red), Fe (olive), Mn (green) and Cu (orange).

The accurate hydrogen adsorption data at low pressures obtained for CPO-27-Cu and -Mn were used to calculate the isosteric heats of adsorption (Q_{st}) of hydrogen for the two materials as a function of loading. The isosteric heats of all the different CPO-27 materials, including Zn-MOF-74, are shown in Figure 6. We obtain a Q_{st} of 8.4 kJ mol^{-1} for CPO-27-Mn (averaged over the first 0.3 molecules H_2 per formula unit and metal site, to minimise the effect of the reduced precision of the values calculated at very low loadings). All these materials display a plateau in the isosteric heat of adsorption plot, before they level off at a loading of about 0.8 H_2 molecules per formula unit (except for Fe, which levels off already at a loading of around 0.6 H_2 molecules per formula unit due to the extreme sensitivity against traces of oxygen of the iron analogue which probably affected the measurement),[10] finally ending up at around 5 – 6 kJ mol^{-1}, which is a typical Q_{st} value observed for H_2 in MOFs without open metal sites.[45] The isosteric heat of adsorption displayed by the manganese (and zinc) analogue show the same trend as the above mentioned CPO-27 materials, albeit with a smoother transition between plateaus, as expected from the smaller energy difference in the binding strengths of the two different types of sites. The most interesting behaviour in the comparison is observed for the CPO-27-Cu material. Whereas all the other materials show an initial plateau in the Q_{st} before it levels off and decreases to around 5 – 6 kJ mol^{-1}, the copper analogue already starts with an initial isosteric heat of adsorption of 6.1 kJ mol^{-1} (averaged over the first 0.3 molecules H_2 per formula unit and metal site), 2.3 kJ mol^{-1} lower than CPO-27-Mn, and remains steady at this level, *i.e.* it already is at the level observed ordinarily for non-open metal site MOFs. This supports the assumption that the two adsorption sites in the copper analogue have equivalent hydrogen affinity. This would explain why the two adsorption sites seem to be filled simultaneously, and the fact that the Q_{st} only starts at 6.1 kJ mol^{-1} confirms that the otherwise strong adsorption effect at the open metal site is negligible when the metal is copper, and that the open metal site is now equivalent in terms of interaction strength to the second adsorption site.

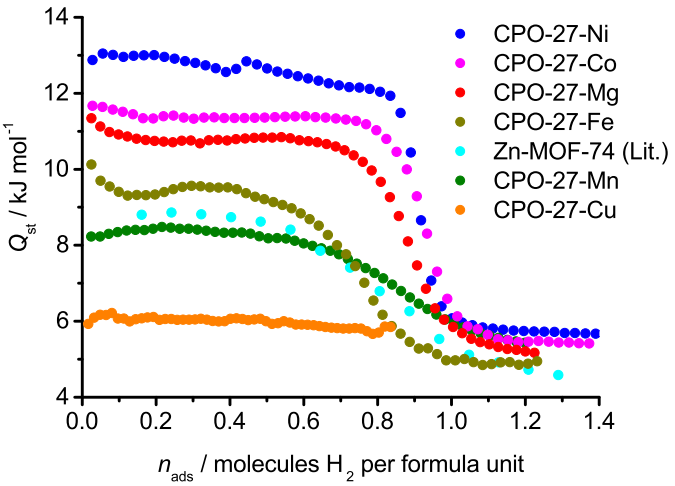

Figure 6: Comparison of hydrogen affinity (quantified as the isosteric heats of adsorption, Q_{st}) for CPO-27-M, where M = Ni (blue), Co (pink), Mg (red), Fe (olive), Zn (light blue), Mn (green) and Cu (orange).

Inelastic neutron scattering spectroscopy and neutron diffraction of H_2 adsorbed in CPO-27-Mn

The INS spectra for different amounts of dihydrogen adsorbed in CPO-27-Mn are shown in Figures 7a and b. At the lowest dihydrogen loading of 0.5 H_2 per Mn centre only two lines at 7.5 and 11.2 meV are observed. As in the previously reported cases,[18,19] these lines originate from the neutron induced para-to-ortho (p-o) first excited rotational state transition of hydrogen molecules adsorbed on the unsaturated metal, here Mn(II), sites. The crystal structure determination from the

neutron diffraction data confirms that only the metal centre site is occupied at this loading (see Figure S6). Compared to the previously measured dihydrogen INS spectra of the Mg, Ni, and Co isostructural materials,[18] in which the corresponding rotational features were observed at 6.7 and 10.2 in Mg, 6.6 and 9.8 for Ni, and 7.7 and 9.6 meV for Co, the centre of gravity of the rotational transitions of H_2 adsorbed on Mn(II) is shifted to higher energies, towards the position of the free rotation at 14.7 meV of molecular hydrogen, suggesting a weaker binding on Mn(II). This spectroscopic observation is in line with the measured isosteric heats of adsorption of H_2 in these materials. Notably, the closest isosteric adsorption heat to that observed for CPO-27-Mn is observed for Zn-MOF-74 (CPO-27-Zn) at 8.8 kJ mol^{-1},[19] with a corresponding p-o rotational transitions observed at 8.3 and 11.3 meV, which is in close proximity to the values reported herein for Mn(II). The intensity of the lines at 7.5 and 11.1 meV increases up to a loading of 0.9 H_2 per Mn. Once the capacity of the metal sites is exceeded at a loading of 1.3 H_2 per Mn, two new features appear at about 10 and 13.8 meV. These are attributed to H_2 molecules located on the adsorption site second in strength (site II), with an approximate adsorption heat of 5-6 kJ mol^{-1} per H_2.[19]

According to our neutron diffraction results the first adsorption site (site I) is located about 2.7 Å from the Mn(II) centre, whilst the second adsorption site (site II) is found in the hexagonal pore corner, near a set of four oxygen atoms within a distance range of 3.3-3.6 Å and a fifth which is still within dispersive interactions range, at about 3.9 Å. Three of the nearest neighbour oxygen atoms belong to a face of the square-pyramidal coordination polyhedron around the manganese atom (Figures 8a and b). The minimum D_2 molecule centre-to-centre intersite distance found here is about 3.2 Å. It should be noted that H_2 sorption on the second adsorption site causes substantial shift of the lowest rotational transition on the metal site, initially observed at 7.5 meV. This is gradually eroded and replaced by a line at 8.1 meV, see Figure 7a. The shift of the line at 7.5 to 8.1 meV is associated with a corresponding upward shift of the higher energy $J = 1$ counterpart from 11.1 to 11.5 meV, also in Figure 7a. At a loading of 2.6 H_2 per Mn, a third peak appears at about 10.8 meV which can be rationalised as arising from H_2 adsorbed on the phenyl ring (the third site to be occupied according to Liu *et al.*,[19] and located with low occupancy in our neutron diffraction results at a loading of 2 D_2 per Mn, Figure 8b). Contrary to the hypothesis by Nijem *et al.*[46] made on the basis of in situ IR studies of hydrogen adsorbed in the isostructural Co(II) containing material, we do not observe significant interactions between H_2 molecules adsorbed on this site and the open metal site. If there were such interactions present in our case, they would affect the position of the rotational lines of H_2 adsorbed on the Mn(II) sites. On the contrary, these rotational lines remain unchanged during further increase of the loading, even up to 4.8 H_2 per Mn (Figure 7b). At this near complete pore filling the corresponding INS spectrum is dominated by a complex broad band at 14.7 meV corresponding to practically free rotation of molecules accommodated in the pore interiors of the material (Figure 7b).

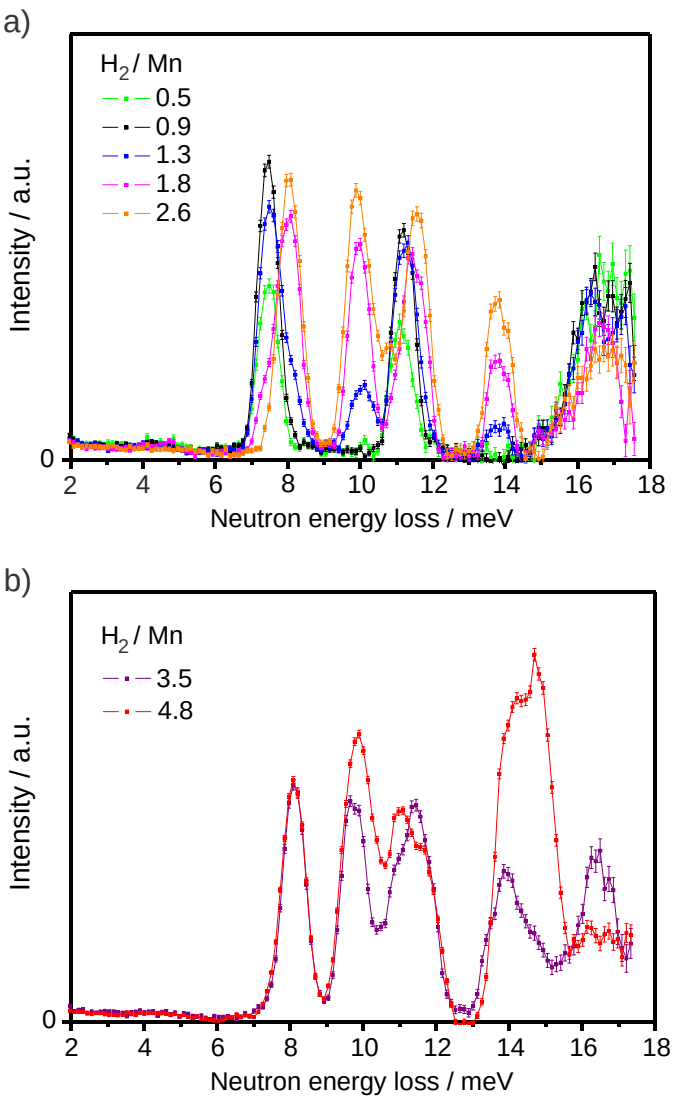

Figure 7: INS spectra for different amounts of dihydrogen adsorbed on CPO-27-Mn.

Inelastic neutron scattering spectroscopy and neutron diffraction of H_2 adsorbed in CPO-27-Cu

INS spectra of a series of H_2 loadings in the Cu material are shown in Figure 9. As might be expected from the sorption associated thermodynamics, there are no features at low energies. At the lowest dihydrogen concentration of 0.45 H_2 per Cu, the adsorbed hydrogen seems to be already distributed over more than one adsorption site with rotational transitions observed at 9.9, 12.8, 14.7, 17.6, and 20.0 meV. Due to the isostructural character of this compound to the other CPO-27 analogues, such as CPO-27-Mn, there is no reason to expect that any other than the open metal site and site II are occupied at such a low loading, as confirmed by the neutron diffraction experiments reported herein. Site I on the open metal site is located about 3 Å away from the Cu(II) ion which is the largest M(II)–D_2 distance yet observed in the series. Site II is located about 3.1 Å from site I, which is within experimental error to the 3.2 Å determined in CPO-27-Mn (Figures 8c and S15).

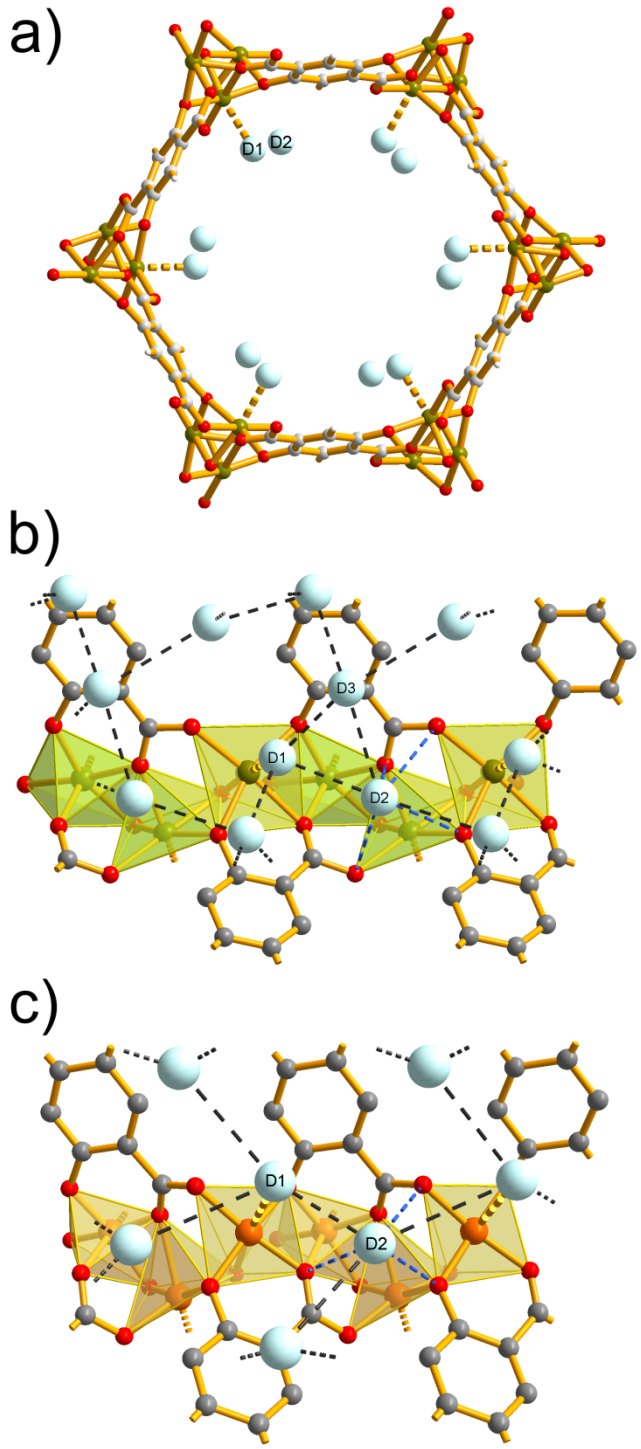

Figure 8: a) Crystal structure of CPO-27-Mn at 20 K showing sites I and II for D_2, viewed along [001]. View of the internal surface of CPO-27-Mn + 2 D_2 showing three partially occupied adsorption sites (b) and CPO-27-Cu + 1.8 D_2 showing two partially occupied adsorption sites (c). As discussed in the experimental section, each deuteron (light blue) represents a D_2 molecule. (Colour scheme: C in grey, O in red, Mn, in olive green, Cu in orange; Hydrogen atoms on phenyl ring are omitted for clarity. Short intermolecular D_2–D_2 distances below 4.1 Å are emphasized by dashed grey lines. Nearest neighbour D_2–O distances below 3.8 Å are emphasized by dashed blue lines.)

However, site II in CPO-27-Cu has only three oxygen atoms in close proximity in the range of 3.3-3.8 Å. In contrast to the previously reported host-guest structures of deuterium adsorbed on CPO-27, the three nearest neighbour oxygen atoms do not belong to a face of the coordination polyhedron around copper. There are two more oxygen atoms at significantly longer distances of 4.2-4.3 Å.

The low H_2 loading INS spectrum may be directly compared to the same for H_2 adsorbed on the coordinatively unsaturated Cu(II) sites in HKUST-1 in which the corresponding lowest energy rotational feature has been observed at about 9.1 meV, originating from H_2 molecules located approx. 2.4 Å from the copper ion,[26,47] about 0.6 Å closer than in CPO-27-Cu (as discussed below). The only change in the INS spectrum upon doubling the hydrogen loading is an overall increase of intensity by a factor of two (Figure 9). It is reasonable to assume that due to the very similar heats of hydrogen adsorption on the Cu(II) open metal site (site I) and site II, the adsorbed hydrogen would be nearly equally distributed over the two sets of sites.

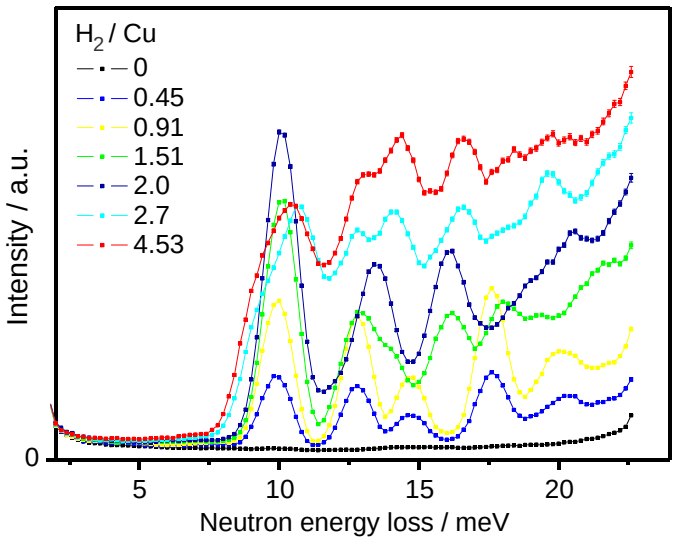

Figure 9: INS spectra of a series of H_2 loadings in CPO-27-Cu.

From the two low-loading spectra in Figure 9, it may be anticipated that a pairwise site occupancy of neighbouring sites I and II does not occur until the loading of 1.51 H_2 per Cu. At this loading, the spectrum is qualitatively changed with two new features at 13.9 and 16.2 meV replacing the 14.7 and 17.6 meV peaks. Although the spectrum is not well resolved, the appearance of H_2 pairs on neighbouring sites I and II at this loading is reflected in the corresponding rotational dynamics of the adsorbed H_2, as in the Mn(II) case. The 13.9 meV line may thus be assigned to H_2 molecules adsorbed at site II with a neighbouring H_2 adsorbed on the Cu(II) site, analogous to the 13.8 meV line in the Mn-compound. Retrospectively, the 14.7 and 17.6 meV lines may be assigned to H_2 molecules adsorbed at site II with no H_2 molecules adsorbed at the neighbouring Cu(II) site. Recall that in the Zn analogue the rotational features of H_2 adsorbed on site II, with the Zn(II) site already occupied, have been observed at 11 meV, 14.5 meV and 19 meV.[19] The Cu(II) sites here are then clearly left with the features seen at

9.9 meV, 12.8 meV and possibly the smaller peak at about 20 meV, which may also arise from combinational roto-vibrational transitions.

The experimentally observed H_2 rotational transitions for site I and II for CPO-27-M are summarised in Table 1. At higher H_2 loading the higher energy $J = 1$ rotational component of H_2 adsorbed at the metal sites moves up in energy due to occupancy of neighbouring sites I and II, as has been observed for the Mn-analogue. At a total loading of 2 H_2 per Cu ion it is merged with the 13.9 meV line, forming a broad feature centred at about 13.4 meV, see Figure 9. Notably, the weak binding of H_2 in CPO-27-Cu leads to the presence of large neutron recoil portion in the spectrum even at these relatively low loadings of 1.5 and 2 H_2 per Cu(II) ion. This is in contrasts to what was observed for the other materials in the series, even in comparison to the Mn(II) analogue which has one of the lowest reported binding energies for H_2, see Figure 7 above.

Table 1: Summary of rotational features site assignments, maximum isosteric heats of H_2 adsorption, and metal site-to-D_2 distances as determined from neutron diffraction data.

CPO-27-M	M(II) site (site I) rotational lines position (meV)□	Site II rotational lines position (meV) □	$Q_{st,\,max}$ (kJ mol^{-1})	d(M–D_2) (Å)	Ref.
Mg(II)	6.7, 10.2	not determined	10.9	2.45(4)	3,18,20
Mn(II)	7.5, 11.2	10.0, 13.8	8.5	2.67(3)	This work
Fe(II)	6.1, 11.5, ~20	10.6, 14.2	9.5	2.53(5)	10,32
Co(II)	7.7, 9.6	not determined	11.5	2.32(2)	18,27
Ni(II)	6.6, 9.8	8, 11	13.5	2.20(1)	17,18,25,27
Cu(II)	9.9, 12.8, ~20	9.9, 14.7, 17.6* 9.9, 14.0, 16.1*	6.1	3.03(2)	This work
Zn(II)	8.3, 11.3, 20.9	11, 14.5, 19.0	8.8	~ 2.6	19

□In the cases where the third line position have not been assigned, only the first two are listed.

*This second set of transitions is inferred from the data obtained with a loading of 1.5 H_2 per Cu.

The spectra of the higher loadings are very much dominated by free recoil appearing as a large hyperbolic background under the rotational features, as previously observed for H_2 adsorbed in activated carbon,[48] for instance. This, along with the absence of clearly resolved new rotational features, indicates very weak binding and disorder for the molecules adsorbed above the capacity of the first two sites. It is essential that the inelastic intensity at about 9.8-10 meV attains its maximum at a total loading of 2 H_2 per Cu, when sites I and II are both occupied, which suggest the competitive filling of the two adsorption sites.

To prove spectrally the thermodynamic equivalence of these two sites, we compared the spectrum of 2 H_2 per Cu to a spectrum of the same material preloaded at 80 K with 1 D_2 per Cu, which was then cooled slowly to 45 K. At this temperature, the same amount of hydrogen gas (1 H_2 per Cu) was added. The corresponding spectrum measured at 4 K is shown in Figure 10, along with the spectrum of 2 H_2 per Cu. The nearly perfect H_2 / D_2 mixing, even at temperatures as low as 45 K, is reflected by the almost shape-identical spectra (Figure 10). It is clear that the two spectra differ only by a scaling factor of approximately two, which is accounted for by the missing scattering intensity of D_2 in the mixed isotope spectrum. This is due to the negligible incoherent inelastic scattering cross-section of deuterium as compared to hydrogen, and corresponding D_2 rotational line shift by a factor of approximately two, caused by the mass of D_2 being twice that of H_2, and hence the rotational constant is decreased by half. Thus the pure D_2 rotational transitions have much weaker intensity and are shifted, leaving only the rotational lines of the H_2 adsorbed on both sets of sites visible.[25,32]

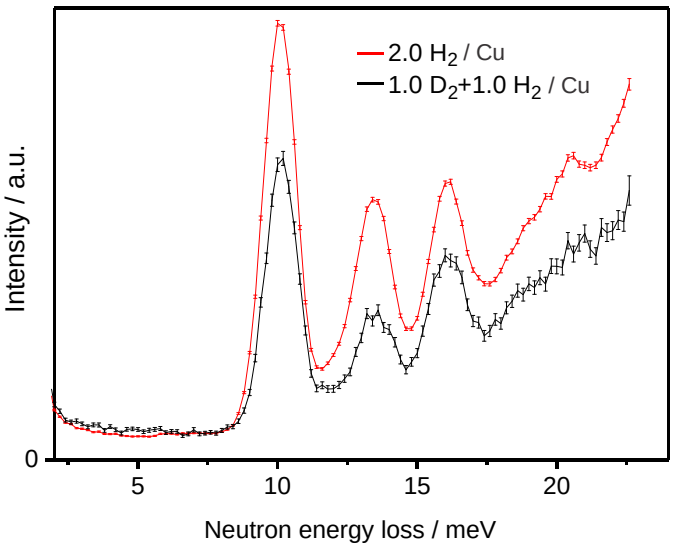

Figure 10: Comparison of INS spectrum of {2 H_2} and {1 D_2 + 1 H_2} loadings in CPO-27-Cu.

In neutron diffraction experiments, especially at high angular range, the use of D_2 instead of H_2 is preferred due to the very large incoherent cross-section of the latter. The crystal structure determinations of D_2 adsorbed on CPO-27-Cu indicate the occurrence of sequential occupancy of the first two adsorption sites when the experiment was performed at 20 K, instead of the parallel occupancy we expected from the sorption and INS experiments. This is likely caused by the fact that D_2 is twice as heavy as H_2. Due to its correspondingly lower zero point energy, pure deuterium is actually able to discriminate better between the two sites, with the isosteric heat of adsorption of D_2 on the open metal site being about 1 kJ mol^{-1} larger than that of H_2.[49,50] As has been recently reported, this effect leads to the CPO-27-M materials having some of the highest selectivity in microporous adsorbents for the separation of D_2 / H_2 isotopes.[49,50] However, also with the use of D_2 instead of H_2, as the temperature is increased the second site

becomes populated before the open metal site is fully occupied. At 55 K and a total loading of 1 D_2 per Cu the ratio of site occupancies decreases to 3:1 in favour of the Cu(II) site.

The Jahn-Teller effect affected Cu(II)–D_2 distance of approx. 3 Å is the longest M–D_2 distance observed in the CPO-27 series, which is also reflected in the weak hydrogen affinity of this compound. The distance is also significantly longer than the Cu–D_2 distance in HKUST-1 of approx. 2.4 Å. The long Cu–D_2 distance in CPO-27-Cu leads to the complete blocking of the adsorption site at the phenyl ring (compare Figures 8b and 8c). The absence of occupation of this third site is further supported by our INS observation of no clearly resolved new rotational features for H_2 loadings above the capacity of the first two sites.

In the Mn compound, a difference of a few kJ mol^{-1} in the isosteric heats of adsorption of site I (the open metal) and site II makes it possible to clearly differentiate between the two different adsorption sites on both macroscopic and microscopic grounds. INS of dihydrogen adsorbed on the CPO-27-Cu framework however, confirms that the energetics of adsorption on the first two sites are very similar.

DFT Calculations

The aforementioned experimental results on the adsorption site thermodynamics are successfully predicted by quantum chemical simulations at the DFT, PBE level, with and without dispersion corrections. The quintessence of these is summarised in Tables 2-4. In Table 2, we present our DFT structural results for CPO-27-Mn and -Cu. The model lattice parameters for the CPO-27-Mn material agree within ~1 % with the neutron diffraction data measured at 10 K, a = 26.33, c = 7.047.[34]

Table 2: DFT, PBE structural data of the two studied materials for the fully desolvated state, for 1 and 2 H_2 molecules adsorbed per metal site. The corresponding values obtained from the Rietveld refinements of the neutron diffraction experiments show good agreement (Table S5).

	Mn		Cu	
	a (Å)	c (Å)	a (Å)	c (Å)
CPO-27-M	26.436	7.133	26.822	6.521
CPO-27-M + 1 H_2	26.437	7.144	26.825	6.512
CPO-27-M + 2 H_2	26.449	7.136	26.824	6.517

Calculated lattice parameters for the Cu-compound are about 4 % larger than the results obtained from our neutron diffraction experiment (Table S5). Notably, our calculations do show a distinct difference in the H_2 binding energies at the Mn open metal site *vs.* site II in the Mn-compound, by 2.4 kJ mol^{-1} H_2 at the pure DFT level and by 5.6 kJ mol^{-1} when dispersion effects are included (Table 3).

Table 3: Calculated site distances and H_2 binding energies, at the PBE and PBE+D level, in the CPO-27-Mn material. For the loading of 2 H_2 per metal centre the individual site II binding energies obtained with respect to the total energy of the corresponding primitive unit cell with 6 H_2 are given, instead of the empty one.

	CPO-27-Mn + 1 H_2		CPO-27-Mn + 2 H_2		
	d(Mn–H) (Å)	E_b (kJ mol^{-1})	d(Mn–H_2) (Å)	E_b (kJ mol^{-1})	d(H_2–H_2) (Å)
PBE	2.69, 2.72	4.5	2.74, 2.67	2.1	3.6
PBE+D	2.64, 2.66	13.9	2.62, 2.62	8.3	3.3
Neutron diffraction	2.67(4)	n.a.	2.63(6)	n.a.	3.18(3)

d(Mn–H) is the distance from the Mn(II) centre to each proton in the nearby H_2 molecule. For the neutron diffraction data, distances given refer to the Mn–D_2 and D_2–D_2 molecule centre minimum distances.

In contrast, whereas the secondary adsorption site in CPO-27-Mn has lower binding energy than the open metal site, the open metal site in the CPO-27-Cu material actually appears marginally weaker than the secondary adsorption site at the pure DFT chemistry level and only stronger by about 2 kJ mol^{-1} when dispersion interactions are included (Table 4). Taking the zero point vibrational energy into account is likely to reduce this difference even further due to the more spacious shape of the oxygen site. It should be noted that for both CPO-27-Mn and CPO-27-Cu, at the pure DFT level of calculation, the distances between H_2 molecules adsorbed at sites I and II, see Table 4, are shorter than the H_2–H_2 distance observed in solid hydrogen (3.8 Å)[51] and similar to the distance for H_2 adsorbed on the graphite surface in the densest incommensurate phase (3.5 Å),[52] and are near the minimum of 3.45 Å of the dimer potential energy curve due to 6 dimensional CCSD(T) calculations.[53] The minimum intersite distance is further decreased by about 0.2-0.3 Å (see Tables 3 and 4) when dispersive forces are taken into account. It is worth noting that such slight adsorbate compression due to adsorbate-adsorbent interactions has been anticipated in most microscopic studies of adsorbed dihydrogen, ranging from different carbonaceous structures to MOFs, including the isostructural MOF-74 compounds.[19,20,25,27,48,54] On average, our calculated dispersion corrected binding energies agree quite well to the experimental isosteric heats of adsorption, especially when taking into account zero-point energy and PV (pressure-volume) term corrections in the enthalpy expression, which amount in total to a downside correction of about 3 kJ mol^{-1}.[55] The calculated difference between the binding energy in the Mn and the Cu-analogues of 2.6 kJ mol^{-1} H_2 (Table 3 and Table 4), corresponds well to the experimental difference between the two isosteric heats of dihydrogen adsorption of 2.3 kJ mol^{-1} H_2.

Table 4: Calculated site distances and H_2 binding energies, at the PBE and PBE+D level, in the CPO-27-Cu material. For the loading of 2 H_2 per metal centre the individual site II binding energies obtained with respect to the total energy of the corresponding primitive unit cell with 6 H_2 are given, instead of the empty one.

	CPO-27-Cu + 1 H_2		CPO-27-Cu + 2 H_2		
	d(Cu–H) (Å)	E_b (kJ mol^{-1})	d(Cu–H_2) (Å)	E_b (kJ mol^{-1})	d(H_2–H_2) (Å)
PBE	2.98, 3.22	3.1	3.08, 3.35	3.2	3.5
PBE+D	2.75, 2.68	11.3	2.68, 2.75	9.4	3.3
Neutron diffraction	3.03(3)	n.a.	3.12(4)	n.a.	3.05(4)

d(Cu–H) is the distance from the Cu(II) centre to each proton in the nearby H_2 molecule. For the neutron diffraction data, distances given refer to the Cu–D_2 and D_2–D_2 molecule centre minimum distances.

Comparing the pure DFT, PBE binding energies and the dispersion interaction corrected energies lead to a conclusion that roughly about half of the binding is due to the latter. It is therefore very important that the dispersion corrections are included for accurate calculations on the dynamics and transition state processes involving H_2 in these materials. Our values seem to match earlier calculations of binding and dynamics of H_2 in the isostructural Zn-based material,[55,56] and substantially improve on recent computational studies involving the whole series of the CPO-27-M (M-MOF-74) structures,[57] except the Cu-analogue for which, to the best of our knowledge, we provide the first theoretical H_2 binding affinity estimate.

In principle, it is possible to also calculate the position of the rotational transitions of adsorbed dihydrogen molecules observed in the INS spectra. This requires computing the adsorption site potential energy surface in at least five dimensions: three translations and two rotations, assuming constant dihydrogen bond length around its adsorption position, as demonstrated for the case of dihydrogen trapped in clathrates,[58,59] and in MOF-5.[60] In the frame of the used quantum chemical models this requires too large computational resource. However, in a simplified model, neglecting the large molecular centre of mass zero point motion, by computing the energy difference between the equilibrium state and the one in which the H_2 molecule is rotated by 90 degrees to an end-on position with respect to the metal centre (see Figure S17 in SI) we are able to estimate the corresponding approximate rotational barrier. In the case of CPO-27-Mn this amounts to about 68 meV while for CPO-27-Cu to 45 meV. These values can be inserted into a simple rotational hindering potential of the form that has been extensively used in many previous parameterisations of the H_2 molecular reorientation in different solids and on surfaces,[48,54,61-64]

$$V_{rot} = \frac{V}{2}(1 - \cos 2\theta),$$

in which V is the rotational barrier height and θ is the angle between the H_2 molecular bond and the basal plane of the square pyramidal unit containing the metal centre, and perturbatively solve the corresponding Schrödinger equation including rotational levels up to $J = 10$. Then the corresponding lowest laying rotational excited states are predicted at about 10 meV for the Mn(II) site and 11 meV for the Cu(II) site. These are in the correct energy range of the observed lines at 7.5 and 11.2 meV for Mn and 10-13 meV for Cu. An accurate model should, however, rely upon more accurate and detailed potential energy surface, and take into account the rotational anisotropy in the plane parallel to the square pyramidal base as well as the large zero point motion of these relatively weakly bound molecules, which in turn presumes significant rotation-vibrational coupling, especially in the case of the CPO-27-Cu.

In two dimensions, the polar and azimuthal angles with respect to the plane of the binding centre and surrounding oxygen ligands, neglecting the molecular centre-of-mass motion and related rotation-translation coupling, the parameterisation has been done for H_2 adsorbed in the vicinity of the Cu(II) centre in HKUST-1,[47] as well as in Zn-MOF-74,[55] also demonstrating modest agreement with the experimental data. In recent work Pham et al. carried out classical potential computational studies on hydrogen sorption in the analogous CPO-27-Mg compound. The isosteric heat of adsorption at the Mg(II) centres is about twice as high as at the Cu(II) centres, hence providing a higher degree of molecule localisation in the adsorbed state, and as a result an excellent agreement between classical potential calculations and experiment has been demonstrated.[65]

Conclusions

We have reported a synthetic procedure for CPO-27-Cu that yields pure material, as identified by powder X-ray diffraction, thermal analysis, and nitrogen gas adsorption.

The most significant result presented herein is the interesting effect that the nature of the metals displays on the hydrogen adsorption properties of the material. For all previous hydrogen sorption measurements on CPO-27 material it has been found that the hydrogen molecules adsorbed at low loadings interact significantly stronger with the metal-organic framework than the successively adsorbed molecules,[18] and that this initial adsorption occurs at the available coordination site of the metal cation, i.e. the open metal site. The trend of the isosteric heats of adsorption for these materials indicates sequential occupation of the two first adsorption sites upon increasing loading with hydrogen, and inelastic neutron scattering (INS) and neutron diffraction experiments have been used to confirm this. A comparison of the Q_{st} data of the CPO-27 materials shows the energy difference between the two different adsorption sites decreases in the order Ni > Co > Mg > Fe > Zn ~ Mn; the hydrogen affinity at the open metal site is much lower for CPO-27-Mn than CPO-27-Ni. Although we already knew that the nature of the metal affect the hydrogen affinity of the framework, we did not expect such a significant

effect when inserting Cu(II) into the framework. The hydrogen affinity at the open Cu(II) site is even lower than that of the Mn version; it is actually so low that sites I and II are equally favourable for H_2 molecules. This conclusion is supported by the hydrogen isotherms, the isosteric heat of adsorption derived from these, DFT model calculations, and inelastic neutron scattering experiments. The Cu(II)–D_2 distance in CPO-27-Cu with its pseudo-octahedral coordination environment is the longest observed in the CPO-27 series, as expected due to the Jahn-Teller effect, and it is also longer than that in HKUST-1 with square-pyramidal copper(II). These results provide an enhanced insight into the impact of the metal cation on the interaction with hydrogen, indicating a potential route to tune the hydrogen uptake capacity in new metal organic framework materials for potential applications. The chemical affinity that is reflected in this very low hydrogen affinity observed for CPO-27-Cu might open up for future interesting separation applications of this material in comparison to the other members of the CPO-27 series.

Acknowledgements

MHR and PDCD acknowledge the support from the Research Council of Norway through the FRINATEK program (221596) and ISP-KJEMI program (grant 209339), and the Laboratory for Electron Microscopy at the Faculty of Mathematics and Natural Sciences at UiB. PAG wishes to acknowledge support from the Project “Beyond Everest" under EU programme REGPOT-2011-1. MF wishes to acknowledge funding from the European Union’s Seventh Framework Programme (FP7/2007-2013) under Grant Agreement No. 290605 (PSIFELLOW/COFUND). This research project was also supported by the European Commission under the 7th Framework Programme through the `Research Infrastructures' action of the `Capacities' Programme, NMI3-II Grants No. 283883. The help of Dr. D. Sheptyakov for taking the HRPT data of the CPO-27-Cu material is greatly acknowledged.

Notes and references

1. R. Saha, B. Joarder, A. S. Roy, S. Manirul Islam and S. Kumar, *Chem. Eur. J.*, 2013, **19**, 16607-16614.
2. F. L. i. Xamena and J. Gascon, eds., *Metal Organic Frameworks as Heterogeneous Catalysts*, Royal Society of Chemistry, Cambridge, 2013.
3. D. Yu, A. O. Yazaydin, J. R. Lane, P. D. C. Dietzel and R. Q. Snurr, *Chem. Sci.*, 2013, **4**, 3544-3556.
4. P. D. C. Dietzel, Y. Morita, R. Blom and H. Fjellvåg, *Angew. Chem. Int. Ed.*, 2005, **44**, 6354-6358.
5. P. D. C. Dietzel, B. Panella, M. Hirscher, R. Blom and H. Fjellvåg, *Chem. Commun.*, 2006, 959-961.
6. P. D. C. Dietzel, R. Blom and H. Fjellvåg, *Eur. J. Inorg. Chem.*, 2008, **2008**, 3624-3632.
7. W. Zhou, H. Wu and T. Yildirim, *J. Am. Chem. Soc.*, 2008, **130**, 15268-15269.
8. N. L. Rosi, J. Kim, M. Eddaoudi, B. Chen, M. O'Keeffe and O. M. Yaghi, *J. Am. Chem. Soc.*, 2005, **127**, 1504-1518.
9. E. D. Bloch, L. J. Murray, W. L. Queen, S. Chavan, S. N. Maximoff, J. P. Bigi, R. Krishna, V. K. Peterson, F. Grandjean, G. J. Long, B. Smit, S. Bordiga, C. M. Brown and J. R. Long, *J. Am. Chem. Soc.*, 2011, **133**, 14814-14822.
10. M. Märcz, R. E. Johnsen, P. D. C. Dietzel and H. Fjellvåg, *Micropor. Mesopor. Mat.*, 2012, **157**, 62-74.
11. R. Sanz, F. Martinez, G. Orcajo, L. Wojtas and D. Briones, *Dalton Trans.*, 2013, **42**, 2392-2398.
12. G. Calleja, R. Sanz, G. Orcajo, D. Briones, P. Leo and F. Martínez, *Catal. Today*, 2014, **227**, 130-137.
13. P. D. C. Dietzel, R. E. Johnsen, R. Blom and H. Fjellvåg, *Chem. Eur. J.*, 2008, **14**, 2389-2397.
14. J. L. C. Rowsell and O. M. Yaghi, *J. Am. Chem. Soc.*, 2006, **128**, 1304-1315.
15. M. Dincă, W. S. Han, Y. Liu, A. Dailly, C. M. Brown and J. R. Long, *Angew. Chem. Int. Ed.*, 2007, **46**, 1419-1422.
16. Y.-G. Lee, H. R. Moon, Y. E. Cheon and M. P. Suh, *Angew. Chem. Int. Ed.*, 2008, **47**, 7741-7745.
17. J. G. Vitillo, L. Regli, S. Chavan, G. Ricchiardi, G. Spoto, P. D. C. Dietzel, S. Bordiga and A. Zecchina, *J. Am. Chem. Soc.*, 2008, **130**, 8386-8396.
18. P. D. C. Dietzel, P. A. Georgiev, J. Eckert, R. Blom, T. Strassle and T. Unruh, *Chem. Commun.*, 2010, **46**, 4962-4964.
19. Y. Liu, H. Kabbour, C. M. Brown, D. A. Neumann and C. C. Ahn, *Langmuir*, 2008, **24**, 4772-4777.
20. K. Sumida, C. M. Brown, Z. R. Herm, S. Chavan, S. Bordiga and J. R. Long, *Chem. Commun.*, 2011, **47**, 1157-1159.
21. P. D. C. Dietzel, R. E. Johnsen, H. Fjellvåg, S. Bordiga, E. Groppo, S. Chavan and R. Blom, *Chem. Commun.*, 2008, 5125-5127.
22. A. C. McKinlay, B. Xiao, D. S. Wragg, P. S. Wheatley, I. L. Megson and R. E. Morris, *J. Am. Chem. Soc.*, 2008, **130**, 10440-10444.
23. H. Wu, J. M. Simmons, G. Srinivas, W. Zhou and T. Yildirim, *J. Phys. Lett.*, 2010, **1**, 1946-1951.
24. W. L. Queen, C. M. Brown, D. K. Britt, P. Zajdel, M. R. Hudson and O. M. Yaghi, *J. Phys. Chem. C*, 2011, **115**, 24915-24919.
25. C. M. Brown, A. J. Ramirez-Cuesta, J.-H. Her, P. S. Wheatley and R. E. Morris, *Chem. Phys.*, 2013, **427**, 3-8.
26. V. K. Peterson, Y. Liu, C. M. Brown and C. J. Kepert, *J. Am. Chem. Soc.*, 2006, **128**, 15578-15579.
27. M. T. Kapelewski, S. J. Geier, M. R. Hudson, D. Stück, J. A. Mason, J. N. Nelson, D. J. Xiao, Z. Hulvey, E. Gilmour, S. A. FitzGerald, M. Head-Gordon, C. M. Brown and J. R. Long, *J. Am. Chem. Soc.*, 2014, **136**, 12119–12129.
28. M. Dincă and J. R. Long, *Angew. Chem. Int. Ed.*, 2008, **47**, 6766-6779.
29. M. P. Suh, H. J. Park, T. K. Prasad and D.-W. Lim, *Chem. Rev.*, 2011, **112**, 782-835.
30. J. Sculley, D. Yuan and H.-C. Zhou, *Energ. Environ. Sci.*, 2011, **4**, 2721-2735.
31. A. G. Wong-Foy, A. J. Matzger and O. M. Yaghi, *J. Am. Chem. Soc.*, 2006, **128**, 3494-3495.
32. W. L. Queen, E. D. Bloch, C. M. Brown, M. R. Hudson, J. A. Mason, L. J. Murray, A. J. Ramirez-Cuesta, V. K. Peterson and J. R. Long, *Dalton Trans.*, 2012, **41**, 4180-4187.

33. E. J. Carrington, I. J. Vitórica-Yrezábal and L. Brammer, *Acta Cryst. B*, 2014, **70**, 404-422.
34. S. J. Geier, J. A. Mason, E. D. Bloch, W. L. Queen, M. R. Hudson, C. M. Brown and J. R. Long, *Chem. Sci.*, 2013, **4**, 2054-2061.
35. S. Janßen, J. Mesot, L. Holitzner, A. Furrer and R. Hempelmann, *Phys. B*, 1997, **234–236**, 1174-1176.
36. T. Unruh, J. Neuhaus and W. Petry, *Nucl. Instrum. Methods Phys. Res. A*, 2007, **580**, 1414-1422.
37. P. Fischer, G. Frey, M. Koch, M. Könnecke, V. Pomjakushin, J. Schefer, R. Thut, N. Schlumpf, R. Bürge, U. Greuter, S. Bondt and E. Berruyer, *Physica B*, 2000, **276–278**, 146-147.
38. P. Fischer, L. Keller, J. Schefer and J. Kohlbrecher, *Neutron*, 2000, **11**, 19-21.
39. J. Rodríguez-Carvajal, *Physica B*, 1993, **192**, 55-69.
40. X. Gonze, B. Amadon, P. M. Anglade, J. M. Beuken, F. Bottin, P. Boulanger, F. Bruneval, D. Caliste, R. Caracas, M. Côté, T. Deutsch, L. Genovese, P. Ghosez, M. Giantomassi, S. Goedecker, D. R. Hamann, P. Hermet, F. Jollet, G. Jomard, S. Leroux, M. Mancini, S. Mazevet, M. J. T. Oliveira, G. Onida, Y. Pouillon, T. Rangel, G. M. Rignanese, D. Sangalli, R. Shaltaf, M. Torrent, M. J. Verstraete, G. Zerah and J. W. Zwanziger, *Comput. Phys. Commun.*, 2009, **180**, 2582-2615.
41. F. Bottin, S. Leroux, A. Knyazev and G. Zérah, *Comp. Mater. Sci.*, 2008, **42**, 329-336.
42. S. Grimme, *J. Comput. Chem.*, 2006, **27**, 1787-1799.
43. J. Rouquerol, P. Llewellyn and F. Rouquerol, in *Characterization of Porous Solids VII*, eds. P. L. Llewellyn, F. Rodriquez-Reinoso, J. Rouqerol and N. Seaton, Elsevier, Amsterdam, Editon edn., 2006, pp. 49-56.
44. F. Rouquerol, J. Rouquerol and K. Sing, *Adsorption by Powders and Porous Solids: Principles, Methodology and Applications*, Academic Press, 1999.
45. W. Zhou, H. Wu, M. R. Hartman and T. Yildirim, *J. Phys. Chem. C*, 2007, **111**, 16131-16137.
46. N. Nijem, L. Z. Kong, Y. G. Zhao, H. H. Wu, J. Li, D. C. Langreth and Y. J. Chabal, *J. Am. Chem. Soc.*, 2011, **133**, 4782-4784.
47. C. M. Brown, Y. Liu, T. Yildirim, V. K. Peterson and C. J. Kepert, *Nanotech.*, 2009, **20**, 204025.
48. P. A. Georgiev, D. K. Ross, P. Albers and A. J. Ramirez-Cuesta, *Carbon*, 2006, **44**, 2724-2738.
49. S. A. FitzGerald, C. J. Pierce, J. L. C. Rowsell, E. D. Bloch and J. A. Mason, *J. Am. Chem. Soc.*, 2013, **135**, 9458-9464.
50. H. Oh, I. Savchenko, A. Mavrandonakis, T. Heine and M. Hirscher, *ACS Nano*, 2013, **8**, 761-770.
51. I. F. Silvera, *Rev. Mod. Phys.*, 1980, **52**, 393-452.
52. M. Nielsen, J. McTague, P. and W. Ellenson, *J. Phys. Colloques*, 1977, **38**, C4-10-C14-18.
53. R. J. Hinde, *J. Chem. Phys.*, 2008, **128**, 154308-154315.
54. P. A. Georgiev, D. K. Ross, A. De Monte, U. Montaretto-Marullo, R. A. H. Edwards, A. J. Ramirez-Cuesta, M. A. Adams and D. Colognesi, *Carbon*, 2005, **43**, 895-906.
55. L. Kong, G. Román-Pérez, J. M. Soler and D. C. Langreth, *Phys. Rev. Let.*, 2009, **103**, 096103.
56. N. Nijem, J.-F. Veyan, L. Kong, H. Wu, Y. Zhao, J. Li, D. C. Langreth and Y. J. Chabal, *J. Am. Chem. Soc.*, 2010, **132**, 14834-14848.
57. P. Canepa, C. A. Arter, E. M. Conwill, D. H. Johnson, B. A. Shoemaker, K. Z. Soliman and T. Thonhauser, *J. Mater. Chem. A*, 2013, **1**, 13597-13604.
58. D. Colognesi, M. Celli, L. Ulivi, M. Xu and Z. Bačić, *J. Phys. Chem. A*, 2013, **117**, 7314-7326.
59. M. Xu, L. Ulivi, M. Celli, D. Colognesi and Z. Bačić, *Phys. Rev. B*, 2011, **83**, 241403.
60. I. Matanović, J. L. Belof, B. Space, K. Sillar, J. Sauer, J. Eckert and Z. Bačić, *J. Phys. Chem.*, 2012, **137**, 014701.
61. T. R. Prisk, M. S. Bryan and P. E. Sokol, *Phys. Chem. Chem. Phys.*, 2014, **16**, 17960-17974.
62. D. White and E. N. Lassettre, *J. Phys Chem.*, 1960, **32**, 72-84.
63. W. J. Stead, P. Meehan and J. W. White, *J. Chem. Soc. Faraday Trans. 2*, 1988, **84**, 1655-1668.
64. W. J. Stead, I. P. Jackson, J. McCaffrey and J. W. White, *J. Chem. Soc. Faraday Trans. 2*, 1988, **84**, 1669-1682.
65. T. Pham, K. A. Forrest, K. McLaughlin, J. Eckert and B. Space, *J. Phys. Chem. C*, 2014, **118**, 22683-22690.

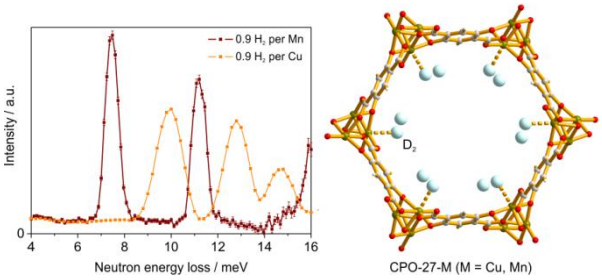

We present a comparative study of hydrogen gas adsorption experiments on CPO-27-Cu and -Mn. The initial isosteric heat of adsorption in CPO-27-Cu is surprisingly low for a material containing open metal sites and in striking contrast to the other members of the CPO-27 series, including the Mn compound, in which the interaction between hydrogen and metal cation is significantly stronger.